Military Technical College
Kobry Elkobbah,
Cairo, Egypt

8th International Conference on Aerospace Sciences & Aviation Technology

COMBINED EFFECT OF SUCTION AND PRESSURE GRADIENT ON SEPARATION OF SUPERSONIC BOUNDARY LAYER

M. A. Elsharnoby *

ABSTRACT

The effect of pressure gradient on separation of supersonic compressible boundary layer is studied at two different Mach numbers of 5.0 and 6.0. Moreover, the study of constant suction effect at different locations is performed for flow at Mach number 5.0. The non-similar boundary layer equations for steady compressible flow have been solved with a potential flow velocity distribution corresponding to power law edge Mach number variation. In this study, the changes in Prandtl number and the specific heat with temperature are considered. The resulting conclusion show that the higher adverse pressure gradient is less affected by a constant suction than the lower one.

1-Introduction

The factors that influence the transition of incompressible and compressible boundary layer flows include pressure gradients, wall roughness, heating or cooling, free steam turbulence, suction or blowing, streamwise curvature, and radiated acoustic noise. The effect of pressure gradients (wall shaping) on laminar flow is of particular interest because it is a passive device for controlling the boundary layers. Previous investigation, have shown that a favorable pressure gradients accelerate the velocity while adverse pressure gradients produce an opposite effect1. The studies in compressible boundary layers are more complicated than in incompressible, the former case is rare, and the most investigations take some restrictions conditions on prandtl number[2], or the relation between the viscosity and tempreature1. Self-Similar solutions for non-zero pressure gradients are rare in compressible boundary layers8, Malik[3] used a self-similar solution do not exist for the investigated conditions. Recently the nonsimilar solutions were studied2 considering the prandtl number and the specific heat as constants.

Flow with suction through a porous wall and cooling are of practical interest. Suction delays both transition to turbulence and boundary layer separation in an adverse pressure gradient. The application of suction at a surface decreases the boundary layer thickness and causes the velocity profile to become more full, that is, the greater the suction, the more deviation of velocity profile from one with inflection point[4].

* Asistant prof., Benha Higher Institute of Technology, Benha, EGYPT.

In this paper the combined effect of suction and pressure gradient on the supersonic compressible boundary layer is preformed. The prandtl number is taken as a function of the temperature; consequently, the results are more accurate from the proceeding calculations. The basic equations in **FD** method are directly applied without any transformation, which make it very easily. The calculations are performed at the end of the boundary layer to complete the stability of compressible boundary layer in the future research.

2- Basic equation

Continuity, momentum, and energy equations in dimensionless form for two-dimensional compressible boundary layer are given respectively by:

$$u_e \frac{\partial \rho F}{\partial x} + \frac{\partial \rho v}{\partial y} + \rho F \frac{\partial u_e}{\partial x} = 0 \qquad (1)$$

$$\rho F u_e \frac{\partial F}{\partial x} + \rho v \frac{\partial F}{\partial y} = \frac{1}{\mathrm{Re}} \frac{\partial}{\partial y}(\mu \frac{\partial F}{\partial y}) + \rho_e \frac{\partial u_e}{\partial x} - \rho F^2 \frac{\partial u_e}{\partial x} \qquad (2)$$

$$\rho F u_e \frac{\partial \theta}{\partial x} + \rho v \frac{\partial \theta}{\partial y} = \frac{1}{R_e} \frac{\partial}{\partial u}(\frac{\mu}{\mathrm{Pr}} \frac{\partial \theta}{\partial y}) + \frac{E_c}{R_e} \frac{u_e^2}{\theta_e} \mu (\frac{\partial F}{\partial y})^2 - \rho_e E_c F \frac{u_e^2}{\theta_e} \frac{\partial u_e}{\partial x} - \rho F \theta \frac{u_e}{\theta_e} \frac{\partial \theta_e}{\partial x} \qquad (3)$$

Where Prandtl number $P_r = \mu_\infty Cp / k_\infty$, Eckert number $Ec = (\gamma - 1) M_\infty^2$, Reynolds number, $Re = u_\infty L / \nu_\infty$, and define $F = u/u_e$, $\theta = h/h_e$.
The boundary conditions for an adiabatic wall are

$$F = 0, \qquad \frac{\partial \theta}{\partial y} = 0, \qquad v = v_\omega \qquad \text{at} \qquad y = 0 \qquad (4\text{-a})$$

In the free stream, the boundary conditions are

$$F \to 1, \qquad \theta \to 1 \qquad \text{at} \qquad y \to \infty \qquad (4\text{-b})$$

In equation (1.4), the subscripts e and refer to the conditions at the edge of the boundary layer and the free stream values respectively, ρ and μ are the non dimensional density and dynamic viscosity coefficient normalized with respect to ρ and μ_∞. The dimensionless velocity components (u, u_e, and V) are normalized with respect to u_∞ Also, the dimensionless enthalpies (h, h_e) are normalized with respect to h_∞. The coordinates x and y are normalized with respect to a reference length L.

In the present work, it is used a certain boundary-layer edge Mach number distribution in the form,

$$M_e = cx^n \qquad (5)$$

Where c is a constant.

The edge temperature is computed using the isentropic flow relation

$$T_e = 1 + \frac{1}{2}(\gamma - 1) M_\infty^2 [1 - u_e^2] \qquad (6\text{-a})$$

The edge velocity distribution u_e derived from Eqn (5)

$$u_e = \frac{M_d}{M_\infty} \sqrt{T_e}\, x^n \qquad (7\text{-a})$$

Where M_d is the desired Mach number at x = 1.0. In these calculations an initial zero pressure gradient is used for length up to x = 0.2, {see Y. H. Zurigat and et. al.[2] 1992.}. From eqns. (6.a) and (6.b), T_e and u_e can be put in the form:

$$T_e = (1 + a)/(1 + ab) \qquad (6\text{-b})$$

$$u_e = \sqrt{b(1 + a)/(1 + ab)} \qquad (7\text{-b})$$

where,

$$a = \frac{Ec}{2} \quad , \qquad b = \frac{M_d^2}{M_\infty^2} x^{2n}$$

M_∞ is calculated from the definition of M_e at x = 0.2 , which is given by the relation, $M_\infty = M_d (0.2)^n$, i.e. M_∞ is dependant on n.

The adiabatic wall temperature, T_w, is calculated from the relation,

$$T_w = 1 + \frac{1}{2}(\gamma - 1) M_e^2 \sqrt{\Pr} \qquad (8)$$

Where Pr in this relation is the taken as constant.

The viscosity coefficient and the coefficient of thermal conductivity are taken as given by Elsharnoby[5](1987) . The viscosity coefficient at $\hat{T}$ >110.4 K , is calculated using the Southland's formula given by:

$$\hat{\mu} = \frac{1.458 \hat{T}^{3/2}}{\hat{T} + 110.4} \times 10^{-6} \qquad \text{kg/ms} \qquad (9)$$

Where $\wedge$ refers to a dimensional quantity. For $\hat{T} \leq$ 110.4 K the viscosity temperature relation is given by :

$$\hat{\mu} = 0.693873 \hat{T} \times 10^{-7} \qquad \text{kg/ms} \qquad (10)$$

For the coefficient of thermal conductivity a similar formula is used, which is given by:

$$\hat{k} = \frac{264.7645\sqrt{\hat{T}}}{1+(245.4/\hat{T})\times 10^{-12/\hat{T}}}\times 10^{-5} \qquad \text{W/mK} \qquad (11)$$

For $\hat{T}$ > 80K, while for $\hat{T} \leq$ 80K, it is used a linear dependence between $\hat{k}$ and $\hat{T}$ which is given by:

$$\hat{k} = (93.33273\times 10^{-6})\hat{T} \qquad \text{W/mK} \qquad (12)$$

3-Solution Technique

Using the implicit finite difference model[6], the equation(3) along with the boundary conditions(4) take the following form,

$$u_{e,m}\left\{\frac{(\rho F)_{m+1,n}-(\rho F)_{m,n}}{2\Delta x}\right\}+u_{e,m}\left\{\frac{(\rho F)_{m+1,n-1}-(\rho F)_{m,n-1}}{2\Delta x}\right\}+\frac{(\rho v)_{m+1,n}-(\rho v)_{m+1,n-1}}{\Delta y}+(\rho F)_{m,n}\frac{\Omega}{\Delta x}\approx 0 \qquad (13)$$

$$(\rho F)_{m,n}u_{em}\left\{\frac{F_{m+1,n}-F_{m,n}}{\Delta x}\right\}+(\rho_e v)_{m,n}\frac{\Delta F1}{2\Delta y}\approx\left\{\rho_{em}-(\rho F^2)_{m,n}\right\}\left\{\frac{\Omega}{\Delta x}\right\}+\left\{\frac{\Delta\mu\Delta F1}{4\,\mathrm{Re}\,\Delta y^2}\right\}+\frac{\mu_{m,n}}{\mathrm{Re}}\left\{\frac{\Delta 2F}{\Delta y^2}\right\} \qquad (14)$$

$$(\rho F)_{m,n}u_{em}\left\{\frac{\theta_{m+1,n}-\theta_{m,n}}{\Delta x}\right\}+(\rho v)_{m,n}\left\{\frac{\theta_{m,n+1}-\theta_{m,n-1}}{2\Delta y}\right\}\approx\left(\frac{\mu}{\mathrm{Pr}}\right)_{m,n}\left\{\frac{\Delta 2\theta}{\mathrm{Re}\,\Delta y^2}\right\}+\left(\Delta\frac{\mu}{\mathrm{Pr}}\frac{\Delta\theta}{4\,\mathrm{Re}\,\Delta y}+\right.$$
$$\left.\frac{Ec}{\mathrm{Re}}\frac{u_e^2}{\theta_e}\right)_m u_{m,n}(\Delta F2)^2\Delta y^2-Ec\rho_e\left(\frac{u_e^2}{\theta_e}\right)_m F_{m,n}\left\{\frac{\Omega}{\Delta x}\right\}-(\rho F\theta)_{m,n}\left(\frac{u_e}{\theta_e}\right)_m\left\{\frac{\theta_{e_{m+1}}-\theta_{e_m}}{\Delta x}\right\} \qquad (15)$$

Where,

$$\Delta 2F = F_{m+1,n+1}-2F_{m+1,n}+F_{m+1,n-1},$$
$$\Delta 2\theta = \theta_{m+1,n+1}-2\theta_{m+1,n}+\theta_{m+1,n-1}$$
$$\Delta F1 = F_{m,n+1}-F_{m,n-1},$$
$$\Delta F2 = F_{m,n}-F_{m,n-1}$$
$$\Omega = u_{e\,m+1}-u_{em}$$

The continuity equation is rearranged to solve for normal velocity at the next mesh point .

$$v_{m+1,n}\approx\frac{(\rho v)_{m+1,n-1}}{\rho_{m+1,n}}-\frac{\Delta y}{\rho_{m+1,n}}\Gamma-\frac{(\rho F)_{m,n}\Delta y\Omega}{\rho_{m+1,n}\Delta x} \qquad (16)$$

Where,

$$\Gamma = u_{em}\left\{\frac{(\rho F)_{m+1,n}-(\rho F)_{m,n}}{2\Delta x}\right\}+u_{em}\left\{\frac{(\rho F)_{m+1,n-1}-(\rho F)_{m,n-1}}{2\Delta x}\right\}$$

The momentum and energy equations are rearranged to give two tridiagonal relations;

$$-\alpha F_{m+1,n+1}+(1+2\alpha)F_{m+1,n}-\alpha F_{m+1,n-1}\approx F_{m,n}-(\beta-\varsigma)\Delta F1+\frac{\Omega}{u_{em}}(\frac{\theta_{m,n}}{F_{m,n}}-F_{m,n}) \qquad (17)$$

$$-\frac{\alpha}{\mathrm{Pr}_{m,n}}\theta_{m+1,n+1}+(1+\frac{2\alpha}{\mathrm{Pr}_{m,n}})\theta_{m+1,n}-\frac{\alpha}{\mathrm{Pr}_{m,n}}\theta_{m+1,n-1}\approx\theta_{m,n}-(\beta-\varsigma)\Delta\theta+Ec\frac{u_{em}^2}{\theta_{em}}\alpha(\Delta F2)^2$$

$$-Ec\frac{u_{em}}{\theta_{e\ m}}\ \Omega\theta_{m,n}-\theta_{m,n}\frac{\Delta\theta}{\theta_{em}} \qquad (18)$$

Where,

$$\frac{h}{h_e}=\frac{\rho_e}{\rho} \quad , \quad \Delta\theta=\theta_{em+1}-\theta_{em}$$

$$\alpha=\frac{\mu_{m,n}\Delta x}{(\rho F)_{m,n}u_{em}\Delta y^2\,\mathrm{Re}} \quad , \quad \beta=\frac{v_{m,n}\Delta x}{2F_{m,n}u_{em}\Delta y}$$

$$\varsigma=\frac{\Delta\mu\Delta x}{(4\rho F)_{m,n}u_{em}\Delta y^2\,\mathrm{Re}} \quad , \quad \xi=\frac{\Delta\frac{\mu}{\mathrm{Pr}}\Delta x}{(4\rho F)_{m,n}u_{em}\Delta y^2\,\mathrm{Re}}$$

$$\Delta\mu=\mu_{m,n+1}-\mu_{m,n-1} \quad , \quad \Delta\frac{\mu}{\mathrm{Pr}}=(\frac{\mu}{\mathrm{Pr}})_{m,n+1}-(\frac{\mu}{\mathrm{Pr}})_{m,n-1}$$

Equations (16),(17), and are to be solved, with the given boundary conditions in equation (4), for the new velocities and temperature. The Tridiagonal matrix algorith[7] is used. In order to carry out the numerical solution, the gas properties must be computed at each step.

The density is calculated from the state equation. Prandtl number and temperature, the NBS table (Hilsenrath et al.[5], 1955) is used. The Prandtl number slightly varies with temperature and the tabulated values are obtained experimentally. The specific heat, C_p, can be computed from the definition of Prandtl number. The tabulated values of the specific heat in turn are used to generate a new table for enthalpy-temperature relation. The adiabatic wall and the edge enthalpies (h_w, h_e) are found from the linear interpolation of the table $h(T)$.

All results are obtained at Re = 3000, $\hat{T}_\infty$ = 120 K, and using double precision arithmetic to attain highly accurate results.

4- Results and Discussions

For the potential flow velocity distribution, Figs1.a and 1b show the streamwise edge Mach number distributions for different values of n at M_d = 5.0 and 6.0. The positive values of n refer to favorable pressure gradients, while, the negative values of n refer to adverse pressure gradients. As shown in these first two figures, M_∞ is greater than M_d for adverse pressure gradients, so it is some difficult to consider the effect of constant suction on the flow near the leading edge; consequently, the calculations could be started at x = 0.5 without arising any problem. On the other hand, the maximum value of x must be chosen such that the point of separation is not behind x = 1.0.

The velocity and temperature distributions across the boundary layer at the location (x = 1.0) are shown in figures 2 and 3 for M_d = 5; while, the same distributions are shown at figures 4 and 5 for M_d = 6. The point of separation for M_d = 5 is found at n = -0.116, but n = -0.115 for M_d = 6. It is noticed clearly that the boundary layer thickness increases for adverse pressure gradient and vice versa. Also BL thickness wider range for M_d = 6 than that for M_d = 5 at the same value of n, which acceptable to the previous results[1].The adiabatic wall temperature increases with increasing M_d , which is in consistence with results in ref.[5].

We discuss the effect of suction that is represented by the normal dimensionless velocity component. at the wall (V_w) . Two different values of uniform suction (V_w = *-0.003, -0.007) at* M_d = 5, are considered. Figures 6, 8, represent the velocity and temperature distributions at the locations x = 0.5, 0.53 respectively for different values of suction. The curves 1, 2 , and 3 correspond to V_w = *0.0 , -0.003, and-0.007* respectively. These figures show that suction prevents the boundary layer separation, and the more suction the more acceleration in velocity and temperature. This result in decreasing of both momentum and thermal boundary layers thickness.

In Figure 7, the curves 1,2,and 3 represents the shift in the point of separation at new locations subjects to the different suction values (V_w 0.0.-0.003, and – 0.007).

While, separation occurs at x = 0.5 for certain adverse pressure gradient (n = -.1332); figure 7 shows that the two non zero values of suction delay the separation in that adverse pressure (n= -0.1332) to occur at x = 0.56,0.72. There are shifts in x = 0.06, 0.22

It is clear From figure 9 that, for M_d = 5 and when there is an adverse pressure gradient (n= -0.1332), separation occurs at x = 0.5. By certain amount of suction (v_w = -0.005), the separation occurs at x = 0.63 . Both momentum and thermal boundary layer thickness become greater at the new point of separation. That is because the flow is exposed to adverse pressure gradient for longer distance. On the other hand, the adiabatic wall temperature decreases due to the decrease in the edge mach number and consuming some energy from the flow by suction.

What have been said about figure 9 could be repeated for figures 10 and 11. From figure 10, the decrease in adverse pressure gradient from n = - 0.1332 to n = - 0.1297, the point of separation without suction is located at x = 0. 55. Applying the same suction (v_w = -0.005) the point of separation is shifted downward to x = 0.74 . For the last figure 11, the point of separation exists at x = 0.6 for adverse pressure with n = -.1268. This separation point is shifted to a new location x = 0.89 when suction with (vw = -0.005) is applied. The shifts in the point of separation in figures 9, 10, 11 are respectively 0.13, 0.19, 0.29 for the same amount of suction.

The same phenomena shown in figure 9, 10 and 11 are obtained from the other calculations. For example, for M_d =5 and adverse pressure (n = -0.131), the suction of V_w = -0.003, -0.007 will shift the point of separation by 0.07,0.3 respectively. These shifts of the point of separation will be equal 0.09, and 0.41, when the adverse pressure decreases (n = -0.12905)

5- Conclusions

From the previous results we find that:

1- The adverse pressure gradient is mainly the source of boundary layer separation.
2- Suction is delaying the supersonic boundary layer separation for all adverse pressure gradients by shifting the location of the separation point downstream.
3- The shift in the location of the point of boundary layer separation increases by increasing suction.
4- The shift in the location of the point of boundary layer separation increases by decreasing the adverse pressure gradient when applying the same value of suction.
5- Supersonic boundary layer flow at higher adverse pressure gradient is less influenced by suction.

6- REFERENCES

[1] Schilchting. H., "Boundary-layer theory", McGraw-Hill (1979)
[2} Zurigat, Y. H., Nayfeh A. H. and Massad, J. A., "Effect of Pressure Gradient on the Stability of Compressible Boundary Layers" . AAIA Journal, vol.30(1992), pp 2204-2211.
[3] Malik, M.R., "Pridica\tion and Control of Transition in Hypersonic Boundary Layers" AIAA Journal. Vol.27 (1989). pp. 1487-1493.
[4] Arnold, M. K., and Chuen-yen C." Foundations Of Aerodynamics", U.S.A,(1976).
[5] Elsharnoby, M. A., "On the stability of Supersonic Boundary Layer" , Ph. D Thesis, Ohio University (1987)
[6] Frank. M. W., " Viscous Fluid Flow" , McGraw Hill(1991.
[7] Anderson, D. A., Tannehill, J. c., and Pletcher, R. H. " Computational Fluid Mechanics and Heat Transfer" , McGraw-Hill book, New York (1984).
[8] Cohen, C. B., and Reshotko, E., "Similar Solutions for the compressible Laminar Boundary Layer with Heat Transfer and Pressure Gradient" , NACA Rept. 1293, (1956).

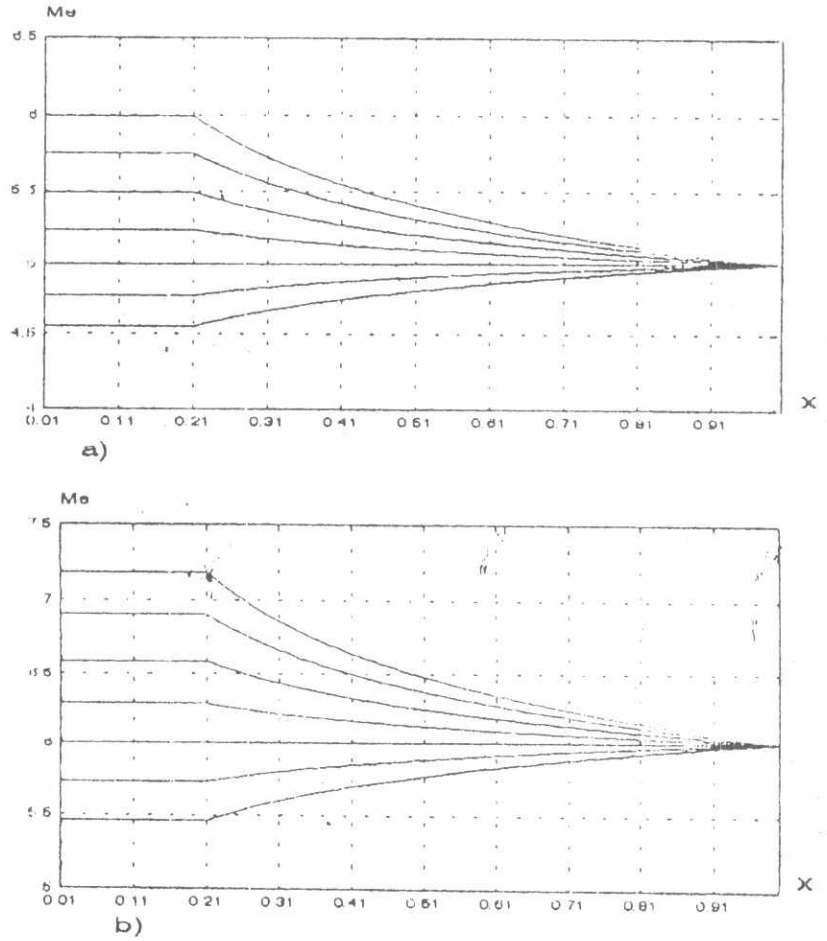

Fig.1 Streamwise distributions of boundary-layer edge Mach number (Me) of pressure-gradient (n);
a) Md=5.0, The values of n, proceeding downward, are -0.116,-0.09,-0.06,-0.03,0.0,0.03, .06 ;
b) Md=6.0, The values of n, proceeding downward, are -0.115,-0.09,-0.06,-0.03,0.0,0.03, .06.

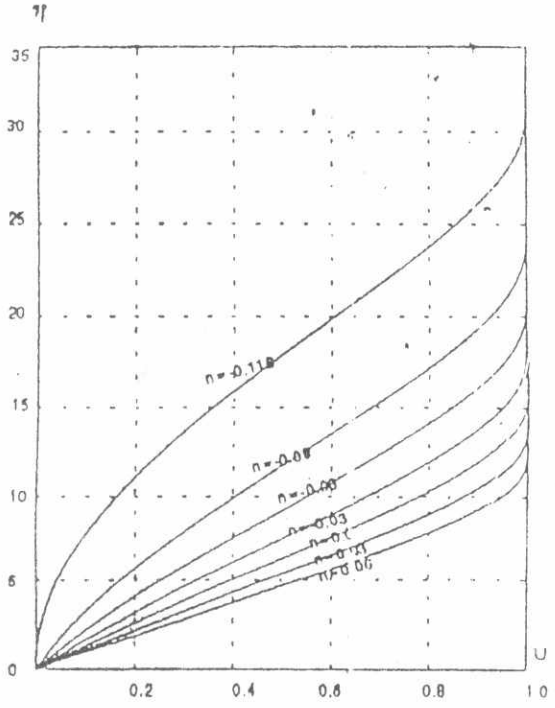

Fig.2 Velocity distributions across the boundary layer for different pressure gradient parameters(Me=5 at x=1.0).

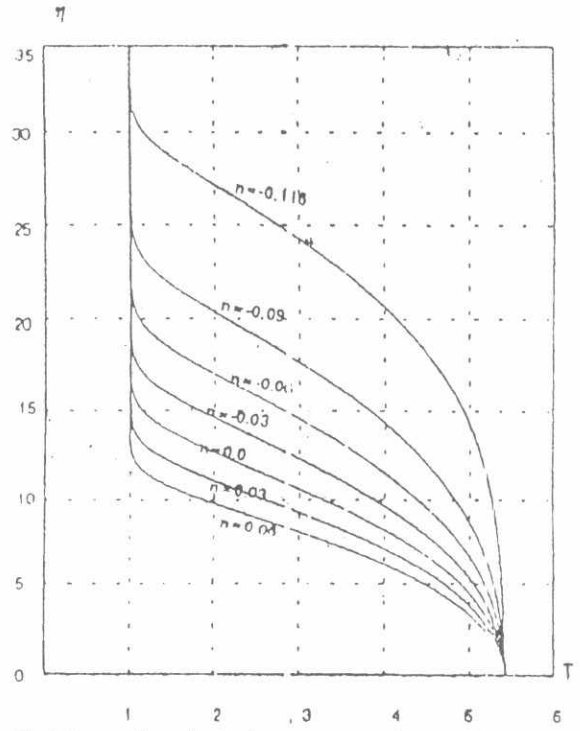

Fig.3 Temperature distributions across the boundary layer for different pressure gradient parameters(Me=5 at x=1.0)

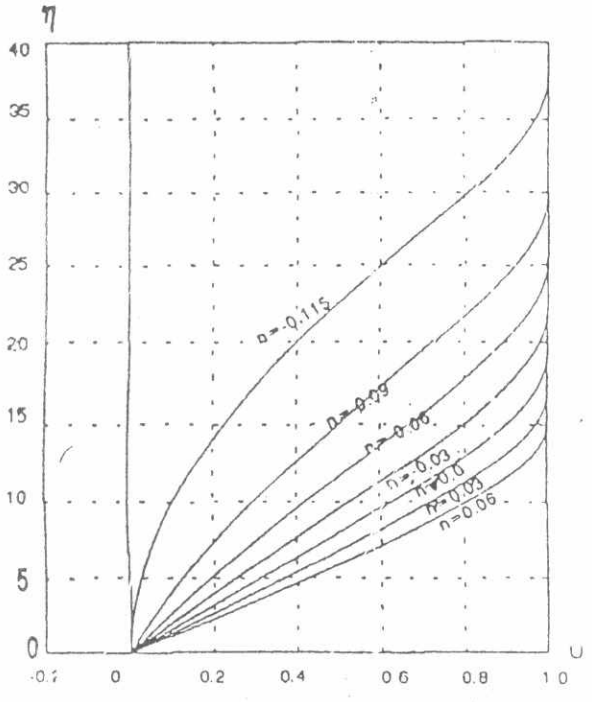

Fig.4 Velocity distributions across the boundary layer for different pressure gradient parameters(Me=6.0 at x=1.0)

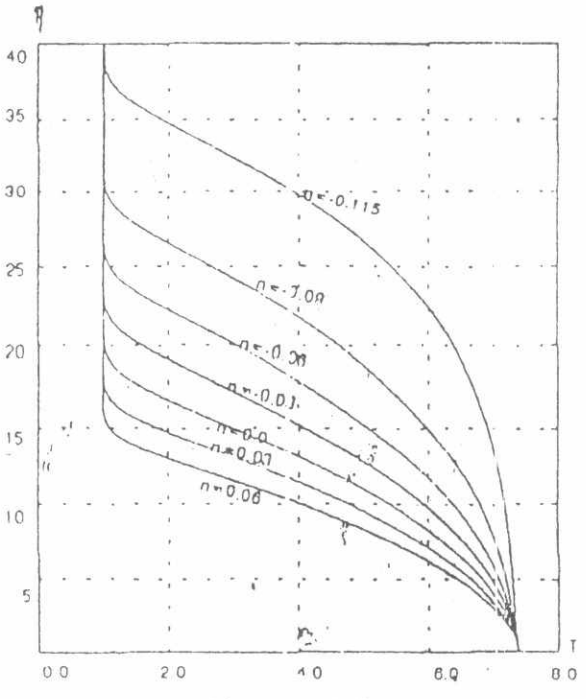

Fig.5 Temperature distributions across the boundary layer for different pressure gradient parameters(Me=6.0 at x=1.0)

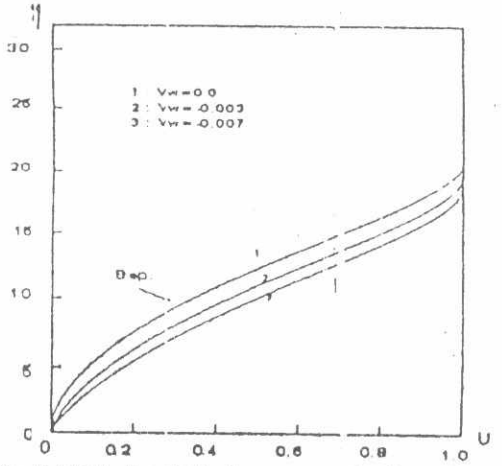

Fig.3(a) Velocity distributions across the boundary layer at x=0.5 for different uniform suction .

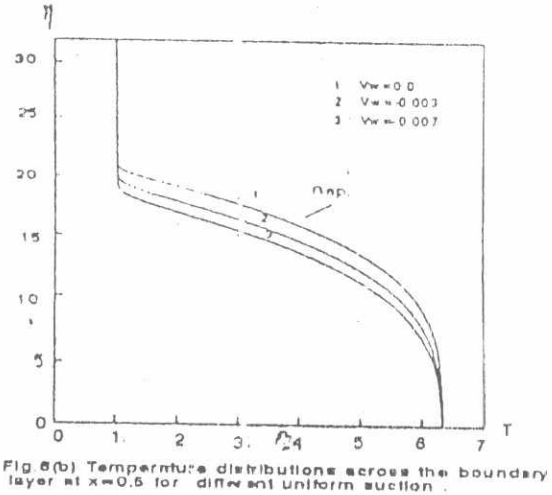

Fig.6(b) Temperature distributions across the boundary layer at x=0.5 for different uniform suction .

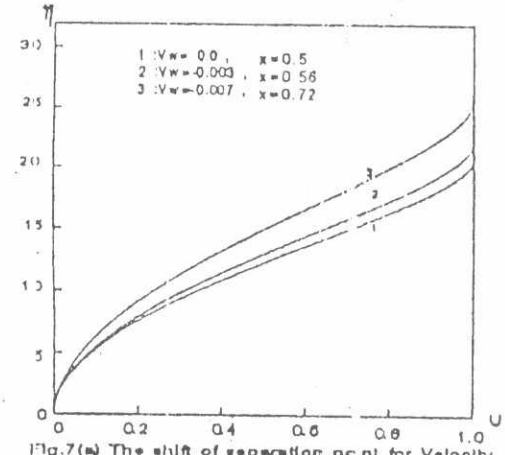

Fig.7(a) The shift of separation point for Velocity distributions across the boundary layer for different uniform suction .

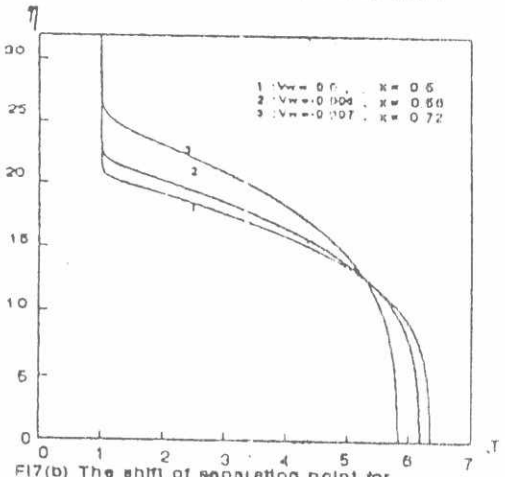

Fig.7(b) The shift of separation point for Temperature distributions across the boundary layer for different uniform suction .

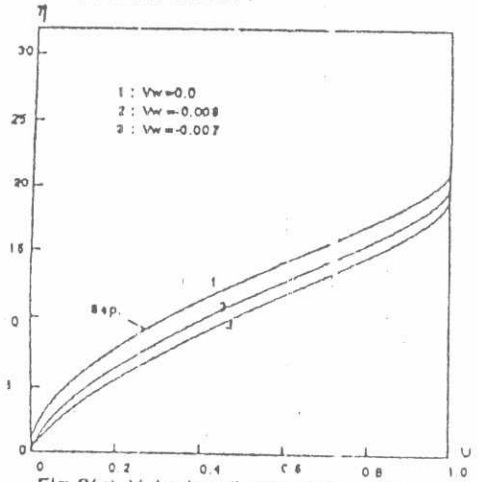

Fig.8(a) Velocity distributions across the boundary layerat x=0.53 for different uniform sucten .

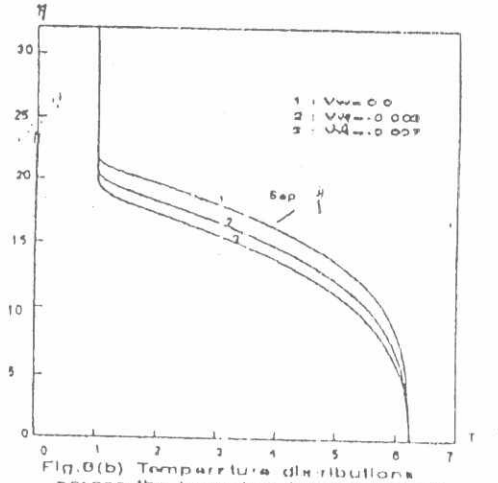

Fig.8(b) Temperature distributions across the boundary layerat x=0.53 for different uniform suction .

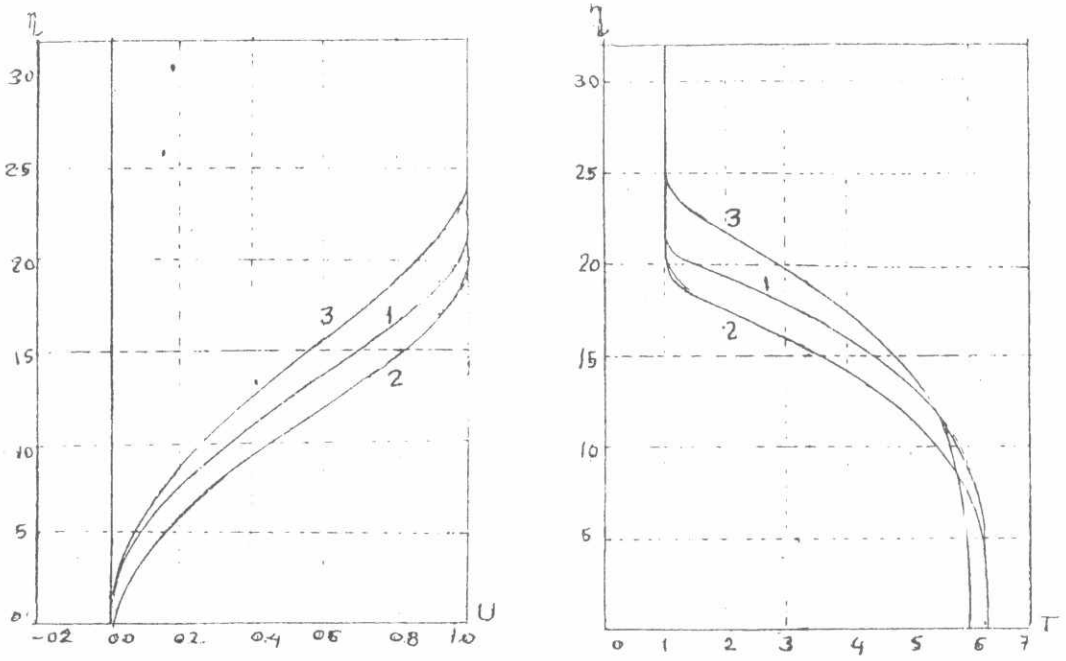

a-Velocity distribution b-Temperature distribution

Fig,9 Effect of Suction on Boundary Layer Separation (M_d = 5.0, n = -0.1332)

1-distribution at point of separation (x = 0.5) without suction.
2-distribution at x = 0.5 with suction (v_w = -0.005)
3-distribution at the new point of separation (x = 0.63) with suction (v_w = -0.005) .

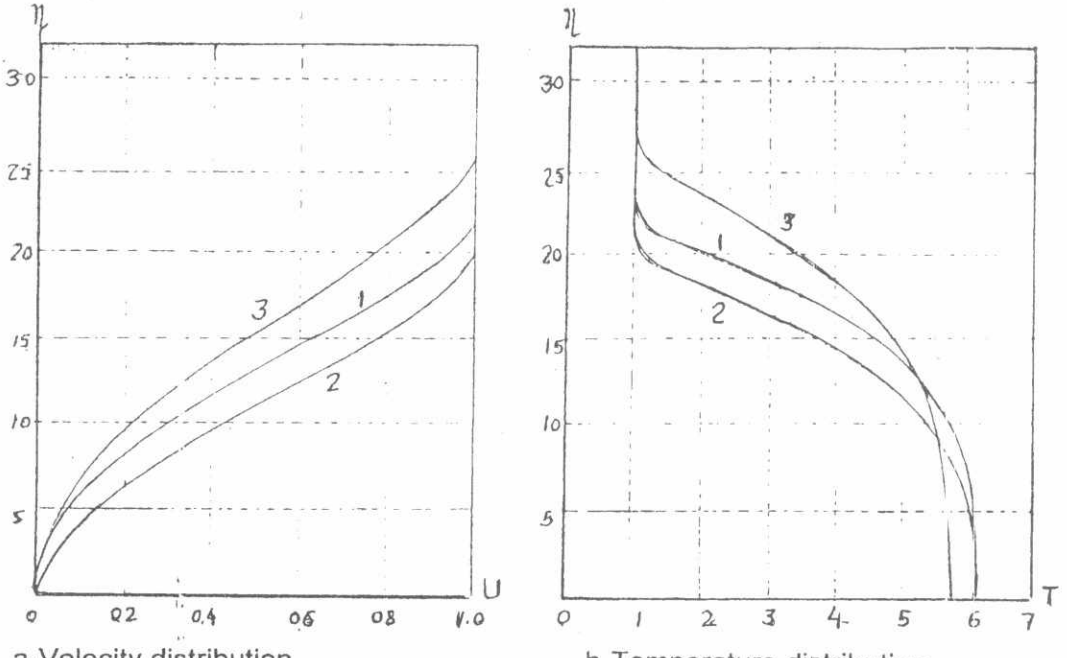

a-Velocity distribution b-Temperature distribution

Fig,10 Effect of Suction on Boundary Layer Separation (M_d = 5.0, n = -0.1297)

1- distribution at point of separation (x = 0.55) without suction.
2- distribution at x = 0.5 with suction (v_w = -0.005)
3- distribution at the new point of separation (x = 0.74) with suction (v_w = -0.005) .

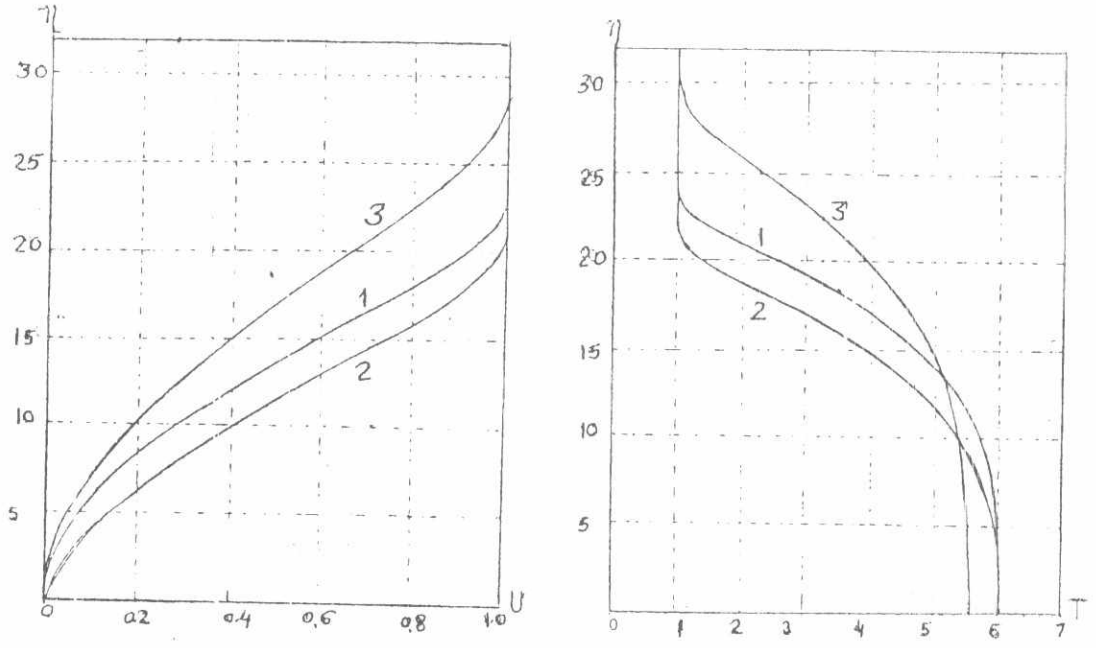

a-Velocity distribution b-Temperature distribution

Fig,11 Effect of Suction on Boundary Layer Separation (M_d = 5.0, n = -0.1269)

1-distribution at point of separation (x = 0.6) without suction.

2-distribution at x = 0.5 with suction (v_w = -0.005)

3-distribution at the new point of separation (x = 0.89) with suction (v_w = -0.005) .